Journal of Catalysis **206,** 230–241 (2002)
doi:10.1006/jcat.2001.3496, available online at http://www.idealibrary.com on IDEAL®

Pore Size Effects in Fischer Tropsch Synthesis over Cobalt-Supported Mesoporous Silicas

Andrei Y. Khodakov,*,[1] Anne Griboval-Constant,* Rafeh Bechara,* and Vladimir L. Zholobenko†

*Laboratoire de Catalyse de Lille, Université des Sciences et Technologies de Lille, Bât. C3, Cité Scientifique, 59655 Villeneuve d'Ascq, France; and †School of Chemistry and Physics, Keele University, Staffordshire ST5 5BG, United Kingdom

Received July 13, 2001; revised November 21, 2001; accepted December 12, 2001

Pore size effects on Fischer Tropsch reaction rates and selectivities over cobalt catalysts were studied at atmospheric pressure using periodic (SBA-15 and MCM-41) and commercial mesoporous silicas as catalytic supports. The catalysts were characterized by nitrogen adsorption, X-ray diffraction (XRD), X-ray photoelectron spectroscopy (XPS), thermogravimetric analysis (TGA), and oxygen titration. Fischer Tropsch reaction rates were found much higher on cobalt catalysts with the pore diameter exceeding 30 Å than on the narrow pore catalysts. A larger diameter of catalyst pores also led to significantly higher C_{5+} selectivities. The catalytic effects were interpreted in terms of different cobalt particle size and reducibility in the wide pore and narrow pore silicas. XRD and XPS showed that the size of supported cobalt species strongly depended on the pore size, increasing with increases in catalyst pore diameter. TGA and oxygen titration indicated higher extent of overall reduction of cobalt species in wide pore supports. Lower reducibility of small cobalt particles is likely to be one of the reasons responsible for the lower Fischer Tropsch reaction rates and higher methane selectivities on narrow pore cobalt catalysts.

Key Words: **Fischer Tropsch synthesis; cobalt catalysts; mesoporous materials; porosity; nanoparticles.**

INTRODUCTION

Fischer Tropsch (FT) synthesis is hydrocarbon production from carbon monoxide and hydrogen. FT synthesis allows making valuable long chain hydrocarbons from relatively cheap natural and associated gas, which are first converted to synthesis gas by vapor reforming and partial oxidation. Rather than burning off unused gas or leaving it untapped, FT synthesis yields products that are useful, cleaner (lower in sulphur and heavier metals than crude oil), easier and cheaper to transport (1, 2). New requirements for the residual sulphur (30–50 ppm) in diesel fuel are a prime reason for renewed interest in FT synthesis in Europe.

FT synthesis proceeds on metal supported catalysts. The efficiency of FT synthesis can be improved by design of new catalysts with higher productivities, higher C_{5+} yields, and lower methane selectivities. A large number of papers published so far focus on optimization of metal function in monometallic (Co, Fe, Ru, Mo) and bimetallic FT catalysts (3–12).

The effect of support and its porosity on FT reaction rate and hydrocarbon selectivities remains, however, still unclear. Mass transport limitations for carbon monoxide and hydrocarbons in catalyst pores, pore filling, and condensation of heavier hydrocarbons, different adsorption properties of metal particles located in narrow and wide pores are often employed to explain the effect of pore sizes on FT reaction rates and selectivities. Anderson *et al.* (13) for example, attributed the observed increase in methane selectivity with decreasing average pore diameter to mass transport phenomenon. It was suggested that greater rate of diffusion of hydrogen inside pores filled with liquid products compared to that of carbon monoxide caused an increase in H_2/CO ratio in catalyst pores, and thus, a shift toward formation of lighter hydrocarbons. Lapszewicz *et al.* (14) showed that variation of product distribution as a function of catalyst pore diameter could be the result of changing adsorption patterns of hydrogen and carbon monoxide rather than mass transfer phenomena. Vanhove *et al.* (15) found that textural properties of Co catalysts supported by alumina could modify the chain length of hydrocarbons. The effect was assigned to different residence times of hydrocarbons in alumina pores due to pore condensation and filling. Bartholomew and Reuel (16) reported strong support effects in carbon monoxide hydrogenation on cobalt catalysts. The order of decreasing CO hydrogenation activity was $TiO_2 > SiO_2 > Al_2O_3 > C > MgO$. The specific activity of cobalt on all studied catalysts also decreased with increasing metal dispersion. Iglesia *et al.* (17, 18) showed that FT specific activity was proportional to metal dispersion and almost independent of the support (SiO_2, Al_2O_3, TiO_2, ZrO_2 modified by SiO_2 and TiO_2). The support was found to slightly influence C_{5+} selectivity due to transport enhanced secondary reactions such as α-olefin readsorption.

Microporous and mesoporous oxides are common supports for metal catalysts. Traditional mesoporous materials

[1] To whom correspondence should be addressed. E-mail: andrei.khodakov@ec-lille.fr.

0021-9517/02 $35.00

are irregularly spaced and their pore sizes are broadly distributed. Thus, it is rather difficult to figure out in which pores Fischer Tropsch synthesis takes places. Moreover, at FT reaction conditions the products, wax and carbon deposits could easily block a part of catalyst pores making them unavailable for reacting molecules. Recently discovered MCM-41 and SBA-15 periodic mesoporous silicas (19–26) represent a new class of inorganic oxides. Their surface areas are approaching 1000 m^2/g, pore size distributions in periodic mesoporous silicas are very narrow. The pore sizes can be adjusted from 20 to 300 Å at the stage of synthesis of these materials using various surfactants and different reaction conditions. Thus, periodic mesoporous silicas can be considered as model supports, which allow the effect of pore size on catalytic behavior of supported catalysts to be studied.

This work addresses the effects of pore size on the structure of Co species and catalytic behavior in FT synthesis of Co catalysts supported by mesoporous silicas. Both periodic and commercial mesoporous silicas are used as catalytic supports. Nitrogen adsorption, X-ray diffraction (XRD), thermogravimetric analysis (TGA), oxygen titration, and X-ray photoelectron spectroscopy (XPS) are used to characterize the catalysts. Characterization and catalytic activity data are compared at relatively low cobalt contents (about 5 wt%). Previously, Reuel and Bartholomew showed (16) that low cobalt loadings provided the best comparison of catalytic supports for Fischer Tropsch catalysts.

EXPERIMENTALS AND METHODS

1. Catalyst Preparation

Si1 sample (MCM-41 type) was prepared using a surfactant with a shorter chain length (C_{12} compared to usual C_{16}) following procedure reported by Matthae *et al.* (21). The material was prepared by mixing 33.06 g of a 25 wt% solution of the surfactant, dodecyl-trimethylammonium bromide (C_{12}TMAB, Aldrich), with 8.42 g of TMAOH, and 1.4 g of 35% ammonia solution. The silica source, 8.81 g of fumed silica (Aldrich) was added with 20.65 g of deionized water so that the final molar ratio was $73.4SiO_2$: 22.8TMAOH : $13C_{12}$TMAB : $7NH_4OH$: $1420H_2O$. The mixture was stirred for 30 min, then kept at 363 K for 72 h, then filtered and washed with water and ethanol. The final product was dried at 363 K for 24 h and then carefully calcined in nitrogen and oxygen to 773 K.

Si2 silica (MCM-41 type) was synthesized as described in Ref. (22). One gram of 28% NH_4OH solution was added to 21 g of 25% solution of cetyltrimethyl ammonium chloride under stirring. This solution was combined with 5.3 g of tetramethylammonium hydroxide pentahydrate (Aldrich, 97%), followed by the addition of 5.6 g of fumed silica (Cab-o-sil M-5, Cabot) and 11.4 ml of water under stirring. The reacting mixture was transferred into a hermetically closed polypropylene flask and heated in an oven at 373 K for 24 h. The resulting gel was washed with distilled water, then dried at room temperature for 24 h and calcined in air at 773 K for 6 h. The rate of temperature ramping was 1°/min.

Si3 sample (MCM-41 type) was synthesized adapting the procedure described in (23). This material was prepared by stirring 38.5 g of 25 wt% cetyltrimethylammonium bromide (CTMAB, Aldrich) solution with 1.28 g of 35% ammonia solution (BDH), 8.64 g of tetramethylammonium hydroxide pentahydrate (TMAOH, Aldrich), 8.95 g of fumed silica (SiO_2, Aldrich), and 43.77 g of deionized water. The final molar ratio was $37.3SiO_2$: 6.6CTMAB : $6.6NH_4OH$: 11.7TMAOH : $678H_2O$. The synthesis mixture was kept at 351 K for 66 h, then filtered and washed with deionized water and ethanol, to remove excess of surfactant before calcination. The final product was dried overnight at 373 K and then carefully calcined in nitrogen and oxygen to 773 K.

Low angle X-ray diffraction patterns (2-theta range from 1.5 to 10°, Cu$K\alpha$ radiation) of the siliceous MCM-41 materials showed an intense peak at ~2.5° and low intensity peaks at 3–6° characteristic of the hexagonal structure of MCM-41.

SBA-15 silicas (Si4 and Si5) were obtained using block copolymer (P123) poly (ethylene glycol)-block-poly (propylene glycol)-block-poly (ethylene glycol), average M_n ca. 5800 (Aldrich, 43,546-5) as a template. To prepare Si4 sample, 6 g of P123 copolymer was dispersed in 45 g of water and 180 g of 2M HCl under stirring. After complete dissolving P123, 12.75 g of tetraethyl orthosilicate (TEOS) were added to the solution.

To synthesize Si5 silica, 90 g of dimethylformamide, 180 g of water, and 180 g of 4M HCl were mixed in a glass flask under stirring. Then 12 g of P123 was dispersed in the resulting solution under stirring. After complete dissolving of P123, 24 g of TEOS were added.

The mixtures used in the synthesis of Si4 and Si5 silicas were kept at 313 K under stirring for 24 h. Then they were transferred to a hermetically closed polypropylene flask and heated in an oven at 373 K for 48 h. The gels were washed with distilled water, dried at room temperature for 24 h, and calcined in air for 10 h using the same procedure as in the synthesis of Si2 silica. The details of synthesis procedures are also available from Refs. (24–26).

Samples Si6 and Si7 were commercial fumed silicas: Aerosil 380 (Degussa) and Cab-o-sil M5 (Cabot), respectively. These materials were agglomerated by wetting and dried in an oven at 393 K overnight.

Cobalt was introduced to silicas by aqueous incipient wetness impregnation using solutions of cobalt nitrate prepared to obtain 5 wt% Co content in the final catalysts (Table 2). The samples were dried in an oven at 373 K overnight and then calcined in the flow of dry air at 773 K for 5 h. The catalysts were pressed and sieved to obtain 200–500 μm size fractions. Co content in the samples was measured by

atomic absorption at the "Service Central d'Analyses du C.N.R.S" (Vernaison, France).

2. Catalyst Characterization

Surface area and pore size distribution. The BET surface area and pore size distribution in mesoporous silicas were measured using nitrogen sorption at 77 K. Prior to the experiments, the samples were outgassed at 473 K for 5 h. The isotherms were measured using a Micrometrics ASAP 2010 system. The total pore volume (TPV) was calculated from the amount of vapor adsorbed at a relative pressure close to unity assuming that the pores are filled with the condensate in liquid state. The pore size distribution curves were calculated from the desorption branches of the isotherms using Barrett–Joyner–Halenda (BJH) formula (27).

X-ray diffraction. XRD patterns were recorded at room temperature by a Siemens D5000 diffractometer using Cu$K\alpha$ radiation. Average Co_3O_4 particle size was calculated from the Sherrer equation (28) using a (440) Co_3O_4 XRD peak at $2\theta = 65.344$. Instrument line broadening was corrected by calibration using a mechanical mixture of bulk crystalline Co_3O_4 and silica.

TGA. The extent of Co reduction in hydrogen was measured using a Sartorius 4102 electronic ultramicrobalance equipped with a controlled atmosphere cell. Co oxidized catalysts (20–25 mg) were placed in a quartz crucible and were dehydrated in dry air at 773 K for 3 h. Then the samples were cooled down to room temperature. After that treatment, the catalysts were heated in a flow of hydrogen from room temperature to 773 K. The rate of temperature ramping was 1°/min. The extent of overall cobalt reduction (**R**, %) was calculated from the weight loss in the atmosphere of hydrogen at 753 K assuming stoichiometric reduction of Co_3O_4 to metallic cobalt. The data were corrected by subtracting weight losses of silica supports treated under the same conditions.

TGA technique used in the present work to measure extents of cobalt reduction was successfully tested for supported Co/Al_2O_3 catalysts in our previous report (29). An excellent agreement was observed between the extents of Co reduction measured by the TGA (temperature ramping of 1°/min) and by magnetic measurements (29).

Reduction of supported Co_3O_4 species in hydrogen has been a subject of a large number of investigations (6, 29–32). It has been shown that all Co_3O_4 crystallites can be reduced to CoO at the temperature range of 473–573 K; the concentration of Co metal phases being controlled by the ease of $CoO \rightarrow Co$ reduction step. Thus, the relative concentrations of Co metal phases in the reduced catalysts can be calculated assuming complete reduction of Co_3O_4 to CoO and partial reduction of CoO to Co metal. On the basis of the stoichiometry of these two reactions, Eq. [1] is suggested to calculate the relative concentration of Co metal phases (**M**, %—percentage of cobalt in metal phases)

$$M, \% = \frac{4\frac{R, \%}{100} - 1}{3} \qquad [1]$$

where **R**, % is the extent of overall reduction and $\mathbf{R} \geq 25\%$.

The relative concentrations of cobalt metal phases are used for calculating FT turnover rates (Table 3).

Oxygen titration. The catalysts were first reduced in hydrogen at 753 K for 5 h followed by purging in flowing helium for 25 min at 723 K to remove any chemisorbed hydrogen; 0.1 ml pulses of oxygen were then introduced to the flow of He at 723 K. The consumption of O_2 by the catalysts was measured by a thermal conductivity detector. The experiments were completed when the detector showed no consumption of O_2.

XPS. XPS spectra were recorded using a Leybold Heraeux LHS 10 spectrometer equipped with a 300 W Al $K\alpha$ source ($h\nu = 1486.6$ eV) operated at 13 kV and 25 mA. The Si2p line (BE = 103.4 eV) from silica support was used as a reference. The measurements were performed at room temperature in high vacuum (10^{-8} Torr). Assuming both uniform distribution of Co particles in catalyst grains and high specific surface area (>100 m^2/g) of the catalysts, the sizes of Co_3O_4 particles can be calculated using a simplified Kerkhof–Moulijn formula [33]:

$$\left(\frac{I_{Co}}{I_{Si}}\right)_{exp} = \left(\frac{I_{Co}}{I_{Si}}\right)_{monolayer} \frac{1 - \exp\left(-\frac{d}{\lambda_{pp}}\right)}{\frac{d}{\lambda_{pp}}}, \qquad [2]$$

where $(I_{Co}/I_{Si})_{exp}$ is the experimental electron intensity ratio for Co2p and Si2p bands, d is the Co_3O_4 particle size, λ_{pp} is the inelastic mean free path (IMFP) of the Co2p photoelectron passing through Co_3O_4 supported phase, $(I_{Co}/I_{Si})_{monolayer}$ is the predicted electron intensity ratio for Co2p and Si2p bands assuming monolayer coverage of silica by Co_3O_4 phase. The value of $\lambda_{pp} = 18.5$ Å for Co2p electrons in Co_3O_4 was calculated using Seah and Dench formula (34). $(I_{Co}/I_{Si})_{monolayer}$ was obtained according to Eq. [3] using FAT mode ($E_0 = 50$) and photoelectron cross section values (σ_{Si}, σ_{Co}) from (35)

$$\left(\frac{I_{Co}}{I_{Si}}\right)_{monolayer} = \left(\frac{n_{Co}}{n_{Si}}\right)_{bulk} \frac{\sigma_{Co}}{\sigma_{Si}} \left(\frac{E_k^{Co}}{E_k^{Si}}\right)^{-0.23}, \qquad [3]$$

where $(n_{Co}/n_{Si})_{bulk}$ is the ratio of bulk atomic concentrations of Co and Si atoms, E_k^{Co} and E_k^{Si} are the kinetic energies of Co2p3/2 and Si2p electrons, respectively. Equation [2] shows that for a given $(n_{Co}/n_{Si})_{bulk}$, $(I_{Co}/I_{Si})_{exp}$ ratio increases with decreasing particle sizes, $(I_{Co}/I_{Si})_{exp}$

ratio close to $(I_{Co}/I_{Si})_{monolayer}$ indicates monolayer coverage of the support by cobalt atoms.

Catalytic experiments. Prior to catalytic experiments, the samples were reduced in a flow of hydrogen at 753 K for 5 h. Catalytic behavior was studied in a fixed bed flow microreactor operating at 463 K and at atmospheric pressure with H_2/CO ratio of 2. The catalyst loadings were typically between 0.6 and 0.7 g. Carbon monoxide contained 5% of nitrogen, which was used as an internal standard. To avoid possible condensation of the reaction products, the reactor and gas transfer lines were placed in an oven and continuously heated at 433 K. The reaction products were analyzed online by gas chromatography. Analysis of CO, CO_2, CH_4, and H_2 were performed using a 13X molecular sieve column and a thermoconductivity detector. Hydrocarbons (C_1–C_{18}) were analyzed by a flame-ionization detector using a capillary HP-PONA column.

RESULTS AND DISCUSSION

1. Catalyst Porosity

The isotherms of nitrogen adsorption and desorption on mesoporous silicas and the corresponding pore size distribution curves calculated using BJH method (27) are shown in Figs. 1 and 2. The BET surface area, total pore volume and average pore diameter are presented in Table 1. The BET surface area in all periodic mesoporous silicas (Si1, Si2, Si3, S4, S5) was higher than 650 m^2/g, whereas the BET surface area of the commercial silicas (Si6, Si7) was much lower (~200–300 m^2/g). The shape of the isotherms of the Si1 and Si2 sample (Fig. 1a) is typical for MCM-41 silicas (19–22). It corresponds to the adsorption of N_2 on the walls of narrow mesopores. The average pore diameter calculated using BJH method was lower than 20 Å. The surface area, pore volume, and average pore diameter of Si1 and Si2 silicas are in good agreement with previous reports (19–22). The lower closure point of the nitrogen hysteresis loop of the isotherm of Si3 silica (Fig. 1a) is situated at a relative pressure close to 0.42. The pore distribution curve of Si3 presented in Fig. 2a exhibits two peaks at 38 and 25 Å. According to Gregg and Sing (36), the peak in the pore distribution curve at 38 Å is likely to be an artifact reflecting the tensile strength effect of the adsorbate. Thus, the average pore diameter of the Si3 silica is about 25 Å.

Nitrogen adsorption isotherms of Si4, Si5, Si6, and Si7 silicas (Figs. 1b and 1c) belong to type IV according to the classification of Brunauer *et al.* (37). Type IV isotherms occur on porous adsorbents possessing pores in the diameter range from 20 to 500 Å. All the isotherms show a reversible part and a type A hysteresis loop at higher pressures. According to De Boer (38), the type A hysteresis loop is associated with the presence of "cylinder shape" pore of rather constant cross section. The P/Po position of the inflection points is related to a diameter in the mesopore range. The

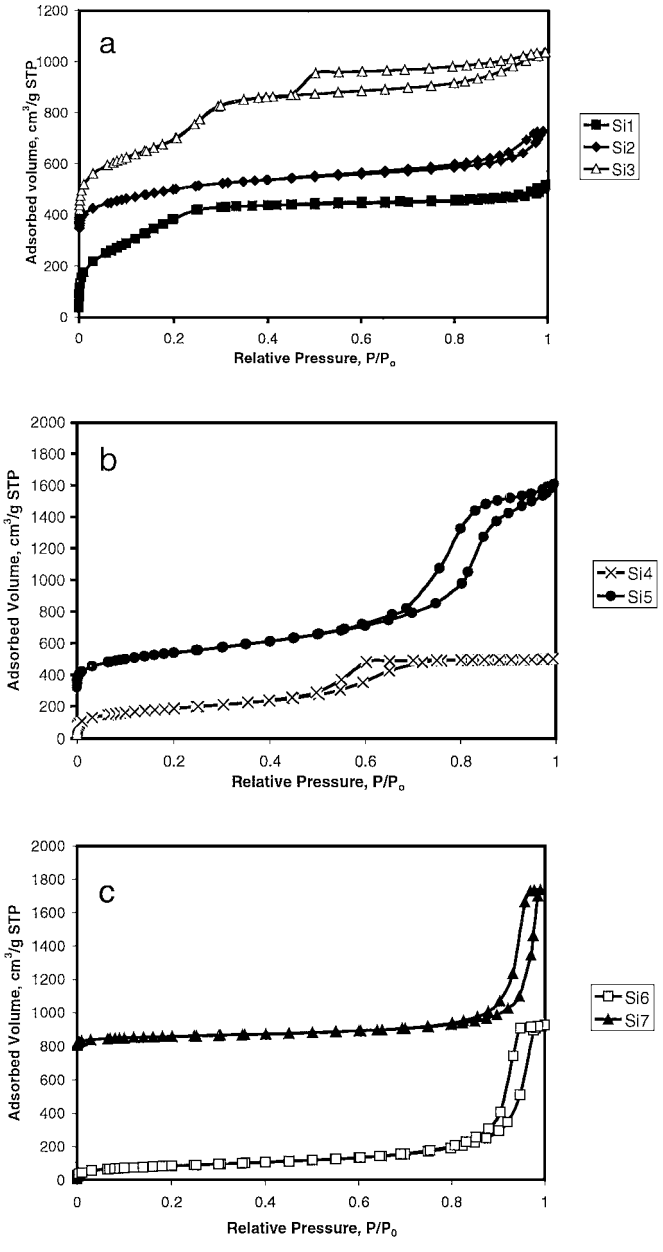

FIG. 1. Nitrogen adsorption–desorption isotherms (a, b, c) of mesoporous silicas. Isotherms of Si2, Si3, Si5, and Si7 silicas are offset for clarity.

BJH pore sizes distribution curves (Fig. 2) were narrower for the Si4 and Si5 periodic mesoporous silicas, than for commercial Si6 and Si7. The average pore diameters ranged from 42 Å in Si4 silica to 330 Å in Si7.

Impregnation of silicas with cobalt nitrate produces a decrease both in specific surface area and in total pore volume (Table 1). At low cobalt loadings (5 wt%) the observed decrease in surface area after catalyst impregnation is primarily attributed to clogging support pores by cobalt species that makes them inaccessible for nitrogen adsorption. This effect was especially pronounced for narrow pore supports

TABLE 1

Adsorption Properties of Mesoporous Silicas and Cobalt Catalysts

	Adsorption properties of mesoporous silicas					Adsorption properties of cobalt catalysts		
Silica	S_{BET}, m^2/g	TPV, cm^3/g	Pore diameter, Å	Synthesis Ref.	Co Catalysts	S_{BET}, m^2/g	TPV, cm^3/g	Pore diameter, Å
Si1	1481	0.75	≈20	(21)	CoSi1	738	0.41	20
Si2	742	0.59	≈20	(22)	CoSi2	462	0.46	≈20
Si3	1285	1.04	25	(23)	CoSi3	397	0.26	20
Si4	679	0.78	42	(25)	CoSi4	586	0.62	43
Si5	887	1.91	91	(26)	CoSi5	674	1.11	75
Si6	311	1.38	280	Aerosil 380	CoSi6	275	1.22	260
Si7	213	0.84	330	Cab-o-sil M5	CoSi7	206	0.76	230

(Si1, Si2, and Si3, Tables 1 and 2). This observation is consistent with previous reports (39–41). Impregnation also leads to a slight decrease in support concentration in modified catalysts, a "dilution effect," which could also contribute to decrease in catalyst surface areas.

Note that the shape of pore size distribution curves remains however the same, though the average pore diameter of the catalysts was smaller after cobalt introduction.

2. *Cobalt Species and Particle Sizes*

The XRD patterns of Co supported catalysts are presented in Fig. 3. XRD patterns characteristic of Co_3O_4 were detected for all oxidized catalysts. The XRD peaks were much broader for Co_3O_4 crystallites in narrow pore silicas (CoSi1, CoSi2, and CoSi3). The Co_3O_4 crystallite sizes (Table 2) were calculated from the widths of XRD peaks (28) using the Sherrer equation ($2\theta = 65.344$ (440)). In the CoSi3 sample, XRD patterns were very broad and had low intensity. This made it impossible to measure the widths of XRD peaks and Co_3O_4 particle sizes for that sample. Table 2 shows that the sizes of Co_3O_4 crystallites depend on the average pore diameters in mesoporous silicas; larger Co_3O_4 crystallites are found in silicas with wider pores.

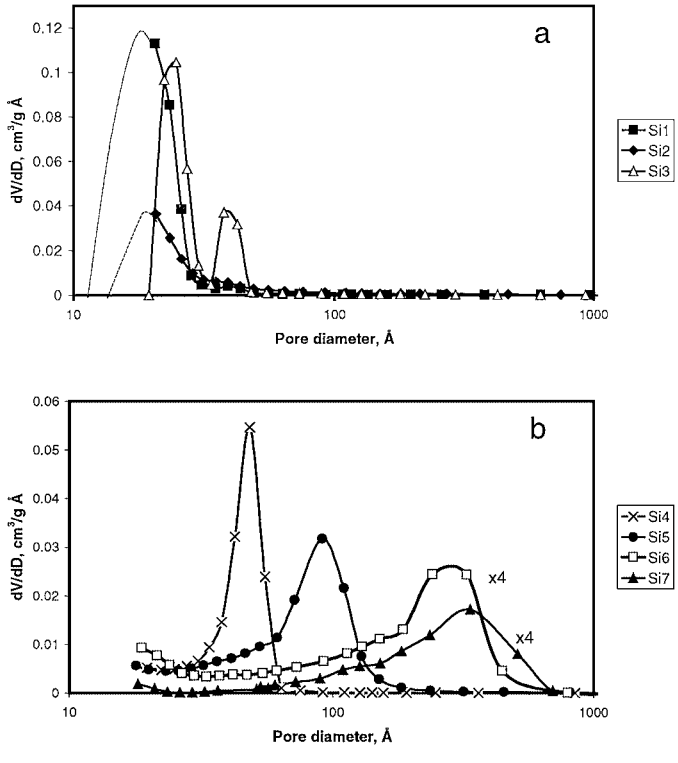

FIG. 2. Pore size distribution curves calculated from nitrogen desorption isotherms for (a) narrow pore and (b) wide pore silicas.

The results of XPS experiments are presented in Figs. 4 and 5 and Table 2. The O1*s* binding energy near 533.1 eV is characteristic of oxygen in SiO_2 (42, 43). Co2*p* XPS spectra (Fig. 4) show that Co_3O_4 is the dominant cobalt phase in oxidized catalysts. This finding is consistent with the observation of Co_3O_4 XRD patterns in all catalysts and our previous X-ray absorption data (44). For wider pore catalysts (CoSi6 and CoSi7) the shapes and binding energies of the Co2*p* line (Fig. 4) were very similar to those of bulk Co_3O_4 (45). Higher intensities of the satellite peak and a shift of the XPS lines toward the higher energy region observed for narrow pore catalysts (CoSi1, CoSi2, CoSi3, CoSi4, and CoSi5), indicate the presence of Co^{2+} ions in interaction with the surface (46).

The sizes of Co_3O_4 particles reported in Table 2 were obtained from the intensity of XPS signal using Kerkhof–Moulijn method (33). The XPS intensity ratio $(I_{Co}/I_{Si})_{exp}$ measured for the different relative atomic concentrations of cobalt $(n_{Co}/n_{Si})_{bulk}$ is presented in Fig. 5. The straight line calculated using formula [3] represents the monolayer limit corresponding to maximum of dispersion of the Co_3O_4 supported phase. Lower relative intensity of Co2*p* XPS experimental signal $(I_{Co}/I_{Si})_{exp}$ indicates large Co_3O_4 particles. The reason for the lower intensity of $(I_{Co}/I_{Si})_{exp}$ signal for larger particles is that a considerable number of Co atoms are located in the bulk of cobalt particles where they are not detectable by XPS (depth of analysis ≈60 Å). Figure 5 and Table 2 show that Co_3O_4 particles are considerably larger

TABLE 2

Characterization of Co Catalysts

Co catalyst	Co content, wt%	Co_3O_4 crystallite diameter from, Å		Estimated cobalt dispersion, %	Extent of overall reduction at 753 K measured by TGA, %	Amount of O_2 consumed in oxygen titration, mole O_2/mole Co
		XRD	XPS			
CoSi1	5.47	57	8	22.5	43.2	0.212
CoSi2	5.67	43	16	29.8	62.9	0.202
CoSi3	5.05	n.d.	18	n.d.	22.8	0.091
CoSi4	6.95	92	70	13.9	72.8	0.373
CoSi5	5.39	121	67	10.6	94.8	0.466
CoSi6	5.75	147	96	8.7	97.2	0.417
CoSi7	4.75	230	76	5.6	94.4	0.673

in wider pore (Si4, Si5, Si6, Si7) than in narrow pores silicas (Si1, Si2, Si3).

Table 2 also shows that Co_3O_4 particle sizes measured from XRD using the Scherrer equation were much larger than those measured by XPS. Similar differences between the sizes of Co_3O_4 particles in silica supported catalysts measured by XPS and XRD were observed in previous reports. Castner *et al*. (47) found for example, that XRD determined Co_3O_4 particle sizes were about 2 times larger than those measured by XPS. These differences seem to be related to the limitations of XPS and XRD methods.

The validity of the Kerkhof and Moulijn model rests on the assumption of uniform distribution of the supported phase between the bulk and outer surface of catalyst grains. Previous works however, showed that impregnation of silicas followed by calcinations could lead to enrichment of Co_3O_4 particles on the exterior of the SiO_2 grains (47). Higher concentration of Co_3O_4 near the outer surface of catalyst grains could lead to higher intensity of the Co2*p*

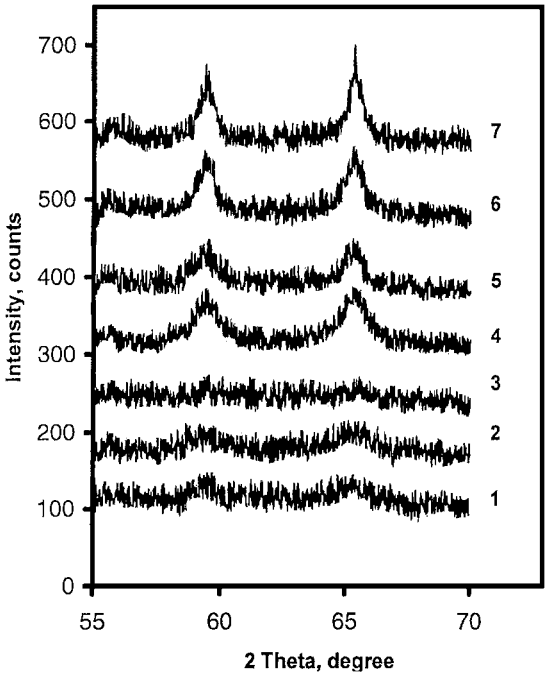

FIG. 3. XRD patterns of Co catalysts: (1) CoSi1; (2) CoSi2; (3) CoSi3; (4) CoSi4; (5) CoSi5; (6) CoSi6; and (7) CoSi7.

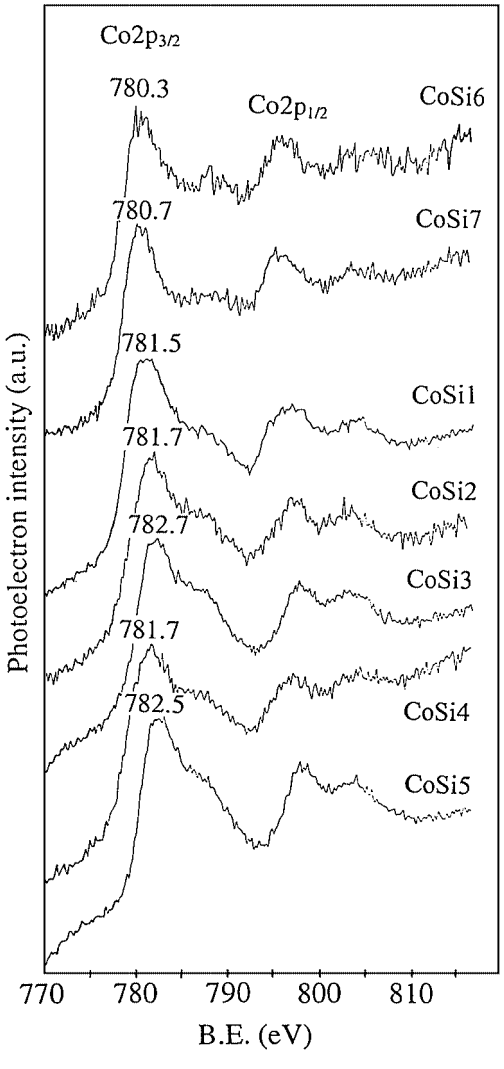

FIG. 4. XPS spectra of the Co2*p* level for Co catalysts supported by mesoporous silicas.

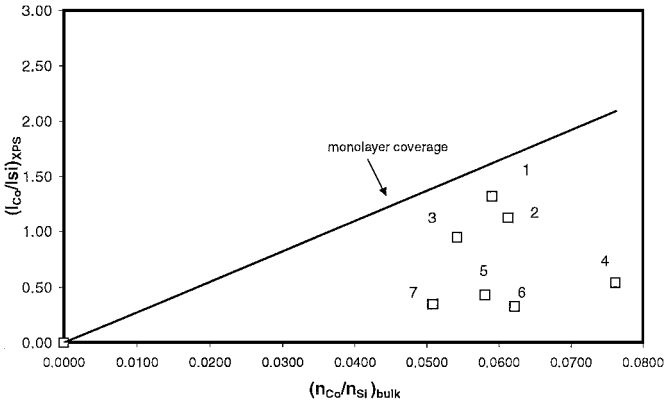

FIG. 5. Relation between measured XPS intensity ratio $(I_{Co}/I_{Si})_{exp}$ and the ratio of bulk atomic concentrations of Co and Si atoms $(n_{Co}/n_{Si})_{bulk}$: (1) CoSi1; (2) CoSi2; (3) CoSi3; (4) CoSi4; (5) CoSi5; (6) CoSi6; and (7) CoSi7.

XPS signal and therefore to underestimating Co_3O_4 particle sizes using the Kerkhof and Moulijn model. The Co_3O_4 particle sizes evaluated from XRD patterns were found slightly larger than the pore diameters of mesoporous silicas (Table 2) probably because of the following reasons. First, the particles of Co_3O_4 could adopt a slightly elongated shape in mesopores. Second, it is known (48) that measuring sizes of crystallites from the half-width of the diffraction profile could slightly overestimate crystallite diameters. Third, some very small cobalt particles could be missed by XRD because of significant XRD line broadening.

Holmen and co-workers showed (7) that Co_3O_4 particle sizes could be converted to the corresponding cobalt metal particle sizes according to the relative molar volumes of metallic cobalt and Co_3O_4. The resulting conversion factor for the diameter (d, Å) of a given Co_3O_4 particle being reduced to metallic cobalt is: $d(Co^0) = 0.75\, d(Co_3O_4)$. Cobalt dispersion ($D$, %) can be calculated from average metal particle sizes (Å) assuming spherical uniform particles with site density 14.6 atoms/nm^2, by the use of formula: $D = 960/d$ (7, 49).

In the present work, the diameter of Co_3O_4 particles measured by XRD is used to estimate Co metal particle sizes and metal dispersions. The estimated values of Co dispersion are shown in Table 2. A reasonable agreement between Co metal dispersions and particle sizes calculated from XRD and from H_2 chemisorption on cobalt supported silica catalysts was previously reported in the literature (7, 18).

3. *Cobalt Reducibility*

Weight loss of the catalysts in hydrogen as a function of temperatures is presented in Fig. 6. The curves exhibit two steps: at 500–600 K and at 600–700 K. In agreement with previous reports (6, 29–32), the weight loss at 500–600 K is attributed to the $Co_3O_4 \rightarrow CoO$ transition. Note that the positions of the first slope in the TGA curves and temperatures of Co_3O_4 to CoO reduction, respectively, are not influenced by Co_3O_4 particle sizes. The second slope at 600–700 K can be assigned to the reduction of CoO phase to metallic cobalt. The position of the second slope in TGA curves depends on the particle size; catalysts containing smaller particles are reduced to metallic cobalt at temperatures higher than those with larger particles. The extents of cobalt reduction at 753 K calculated from TGA data are shown in Table 2. The extent of reduction was significantly lower for narrow pore CoSi1, CoSi2, CoSi3, and CoSi4 than for wider pore CoSi5, CoSi6, and CoSi7 samples.

The amount of oxygen required to oxidize reduced Co species was measured by oxygen titration at 723 K (Table 2). This technique, often based on the assumption of stoichiometric oxidation of metallic cobalt to Co_3O_4 is commonly used to evaluate the extent of Co reduction (7, 18, 50). Recently, we showed (31) that in inert atmosphere at temperatures higher than 623 K supported CoO phase could be more stable than Co_3O_4. Decomposition of supported Co_3O_4 particles to CoO was observed for example, on heating Co supported silica samples in inert atmosphere (31). Therefore, oxygen titration conducted in helium could result in oxidation of Co metal phases to CoO instead of Co_3O_4 or to the mixture of CoO and Co_3O_4. Thus, we believe that O_2 titration assuming selective formation of Co_3O_4 upon oxidation provides underestimated extents of the overall reduction relative to TGA method. O_2 titration data are used in this work qualitatively in conjunction with more reliable values of extents of reduction measured by TGA. Table 2 shows higher consumption of oxygen by wide pore cobalt catalysts in agreement with higher extents of reduction measured by TGA.

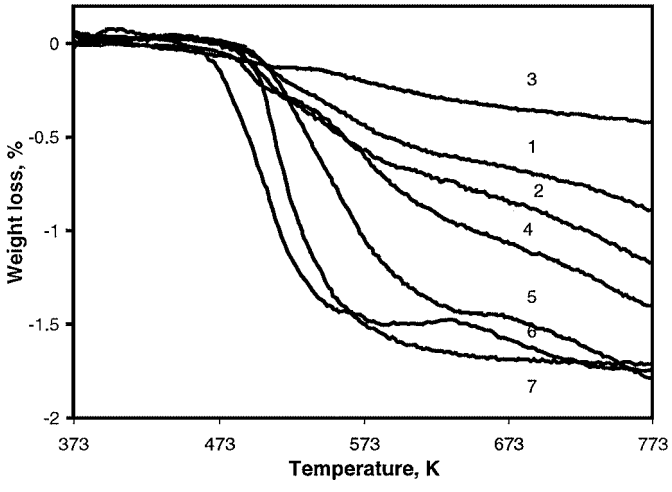

FIG. 6. Weight loss of catalysts in hydrogen: (1) CoSi1; (2) CoSi2; (3) CoSi3; (4) CoSi4; (5) CoSi5; (6) CoSi6; and (7) CoSi7. The curves were corrected by subtracting contributions of supports and normalized to 5 wt% loadings.

4. Catalytic Behavior

Catalytic measurements were made in a differential catalytic reactor, carbon monoxide conversion was lower than 5%. C_1–C_{18} hydrocarbons and water were detected as reaction products. Carbon dioxide was not observed at the reaction conditions.

Figure 7 shows FT reaction rate, methane, and C_{5+} selectivites as functions of time on stream on the CoSi4 sample. FT reaction rates decrease slowly with time-on-stream, whereas hydrocarbon selectivities remain unchanged. After 7 h on stream the reaction rates decreased by about 10–15% relative to the initial values. The catalytic behavior of FT catalysts is usually evaluated in the literature (7, 15–18, 46, 51) using quasi steady state reaction rates and selectivities. It was shown previously (46) that a quasi steady state for Co silica supported catalysts at similar FT reaction conditions could be normally reached after 4 h on stream. Thus, the reaction rates were calculated from carbon monoxide conversions after 7 h on stream and gas hourly space velocities; then they were normalized by the number of cobalt atoms loaded in the reactor. The FT turnover rates (reaction rates normalized by the total number of Co atoms on the surface of metal particles) were obtained from FT reaction rates, relative concentrations of cobalt metal phases calculated using Eq. [1], and cobalt dispersion (Table 3). Co dispersion (Table 2) was calculated from XRD Co_3O_4 particle size using the formulas from Ref. (7).

The hydrocarbon selectivities were calculated on carbon basis. The chain growth probabilities, α, were calculated from the slope of the curve $\ln(S_n/n)$ versus n, where n is the carbon number of the hydrocarbon and S_n the selectivity to corresponding hydrocarbon (52). The catalytic data for the Co catalysts supported by mesoporous silicas are presented in Table 3. Typical hydrocarbon distributions are presented in Fig. 8.

Figure 9 and Table 3 show that the catalytic behavior of Co catalysts supported by mesoporous silicas is strongly affected by porous structure of the support. The reaction rates increase several times as the pore size increases from 20 to 330 Å. The catalysts with pore diameter smaller than 30 Å exhibit low activity, a significant increase in FT reaction rates is observed as the pore size increases to 40 Å. Considerably higher methane (30%) and lower C_{5+} selectivities were observed on narrow pore silicas, whereas the chain growth probabilities (α) were in the range of 0.66–0.78 for both narrow and wide pore catalysts.

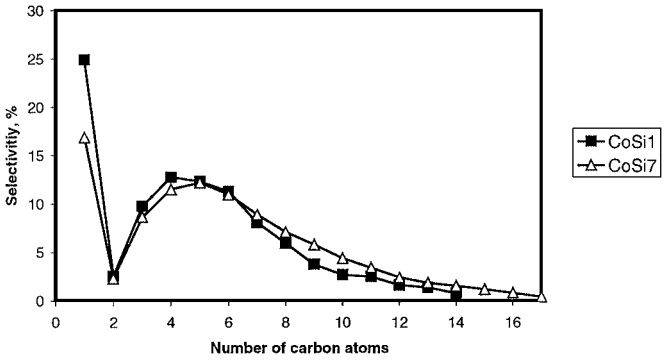

FIG. 8. Typical product distribution on CoSi1 and CoSi7 catalysts ($T = 463$ K, $H_2/CO = 2$, time-on-stream = 7 h).

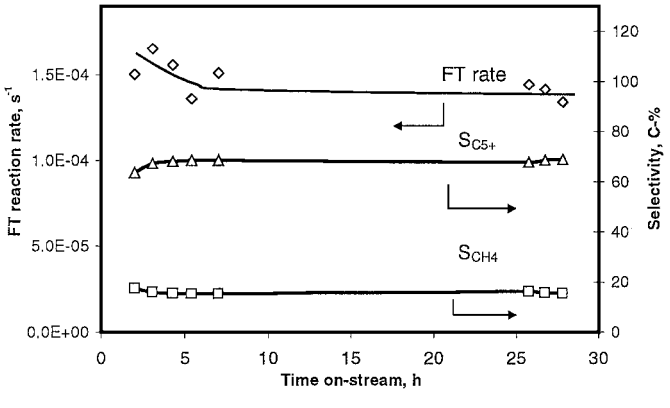

FIG. 7. FT reaction rate, methane, and C_{5+} selectivites as functions of time on stream on CoSi4 sample ($T = 463$ K, $H_2/CO = 2$).

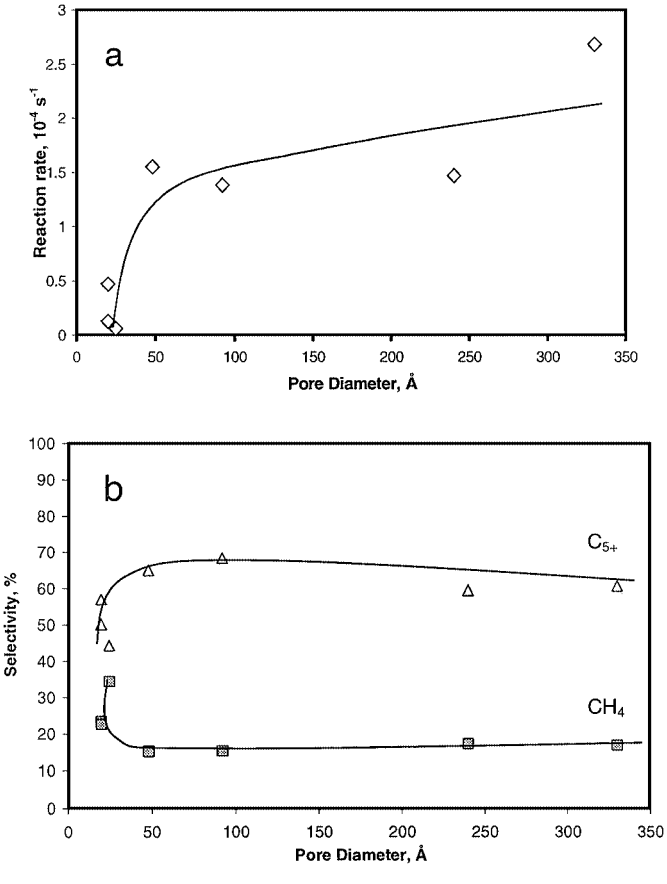

FIG. 9. (a) FT reaction rates and (b) hydrocarbon selectivities as functions of support pore sizes.

TABLE 3

Catalytic Behavior of Co Catalysts Supported by Mesoporous Silicas ($H_2/CO = 2$, P = 1 bar, $T_r = 463$ K, 7 h On-Stream, Conversion <5%)

Co catalyst	Reaction rates, 10^{-4} s^{-1}	Turnover frequency, 10^{-4} s^{-1}	CH_4 selectivity, C-%	C_{5+} selectivity, C-%	α
CoSi1	0.5	9.16	24.9	50.1	0.66
CoSi2	0.1	0.66	22.7	57.0	0.78
CoSi3	0.05	—	34.5	44.4	0.71
CoSi4	1.55	17.50	15.2	65.0	0.74
CoSi5	1.38	13.99	15.3	68.4	0.77
CoSi6	1.47	17.55	17.2	59.5	0.73
CoSi7	2.68	51.72	16.9	60.7	0.70

5. *Pore Size Effects on the Structure of Cobalt Particles and Their Catalytic Performance in FT Synthesis*

Characterization results show that the structure, reducibility of supported cobalt species, and their catalytic behavior are strongly influenced by catalyst porosity (Table 2). The size of supported Co_3O_4 particles measured by both XRD and XPS is found to depend on pore sizes, smaller Co_3O_4 particles being observed in narrow pore silicas.

The dependence of Co_3O_4 particle sizes on catalyst pore diameters (Table 2) suggests preferential localization of Co_3O_4 particle in silica pores. Previous studies have shown that narrow pore size distribution in periodic mesoporous silicas could stabilize supported nanoparticles. Zhang *et al.* (53) reported the procedure to prepare nanosized ZnS particles in ordered mesoporous silicas. Iwamoto *et al.* (54) showed that MCM-41 materials could stabilize nanoparticles of iron oxides. MCM-41 and SBA-15 mesoporous materials were also used (55, 56) to fabricate nanowires of noble metals encapsulated in silica pores. In line with these reports we found that the sizes of Co_3O_4 particles in mesoporous silica are controlled by pore sizes.

Differences in Co_3O_4 particle sizes lead to differences in cobalt reducibility. Much lower reducibility of small Co_3O_4 particles in narrow pore supports was observed by TGA. The extents of reduction vary from 20–60% for narrow pore silicas (Si1, Si2, Si3) to 90–100% for wider pore supports (Table 2). A lower consumption of oxygen by CoSi1, CoSi2, and CoSi3 catalysts measured by oxygen titration also indicates a lower extent of reduction of Co species in narrow pore silicas. It can be suggested therefore, that small cobalt particles in narrow pores are more difficult to reduce than larger particles in wider pores. This suggestion is consistent with earlier data (6, 29–32). It is known that reducibility of Co_3O_4 crystallites depends on their sizes; the ease of reduction increasing from smaller to larger particles. It was suggested (31) that interaction between metal and support in smaller particles was much stronger than in larger particles and this interaction was likely to stabilize small oxidized particles and clusters in silica. We found that the sizes of supported Co_3O_4 crystallites are controlled by support pore diameters in mesoporous silicas. Larger pore diameters lead to larger Co_3O_4 particles. The reducibility of Co species is higher in larger pore silicas, because larger pore silicas contain larger, and thus easier to reduce, Co_3O_4 crystallites.

Thus, silica porosity affects the structure of Co supported species in two ways: first, the support pore diameter controls the size of encapsulated Co species; second, cobalt reducibility is influenced by support porosity; reducibility of cobalt species being much lower in narrow pore supports.

Let us now discuss the effect of pore size on the catalytic behavior of Co supported mesoporous silicas. Catalytic data show that FT reaction rates were much lower on Co catalysts supported by narrow pore materials. Catalyst characterization revealed that narrow pore catalysts contained smaller cobalt particles. Thus, the activity of the catalysts seems to be affected by the size of cobalt particles. The FT turnover rates estimated from FT reaction rates, relative concentrations of cobalt metal phases and dispersion, were also found to be lower for smaller particles than for larger particles (Table 3).

These results are in agreement with previous findings. Reuel and Bartholomew (16) found that turnover frequencies of Co/Al_2O_3, Co/SiO_2, Co/TiO_2, and Co/C catalysts prepared by impregnation method increased with decreasing metal dispersion. The trend of decreasing activity with increasing dispersion was assigned either to changes in surface structure with decreasing particle size or to electronic modifications as a results of more intimate interactions of the small crystallites with the support. It was also suggested (51) that FT synthesis was structure sensitive and favored sites to which CO was strongly coordinated. Since only partially reduced Co samples were studied in that work, it was rather difficult to draw unambiguous conclusions about structural sensitivity of FT synthesis. Iglesia *et al.* (17, 18) showed that FT synthesis rates were proportional to metal dispersion and were independent of the support. They attributed lower activity of small cobalt particles observed in previous reports to the differences in the extent of reduction as a function of metal dispersion, chemical identity, and surface properties of the support. It was suggested that partially reduced cobalt species did not catalyze FT synthesis and that small particles could be easily reoxidized by water and other reaction products at the conditions of FT synthesis. Note that it is rather difficult to separate catalytic effects which could arise from possible reoxidation of small Co particles at FT reaction conditions or from structural sensitivity of FT synthesis over Co particles of different sizes.

Our data are consistent with the suggestion that lower activity of small cobalt particles could be attributed to their

lower reducibility. Lower FT catalytic activities were always observed on partially reduced cobalt species. Tables 2 and 3 show that FT reaction rates and turnover frequencies increase dramatically as the extents of reduction reach 90%. It is also seen that FT turnover frequencies, which represent FT reaction rates normalized by the number of available Co surface atoms, increase with increasing Co particle sizes. The dependence of FT turnover frequencies on Co particle sizes suggests either possible reoxidation of smaller cobalt particles at FT reactions conditions or structural sensitivity of FT synthesis.

Table 3 displays higher methane selectivity on smaller cobalt particles located in narrow pore silicas. Methane selectivity drops from 30 to 15% as silica pore sizes increases from 20 to 100 Å. Previous studies also report higher methane selectivity on small Co particles. At least three suppositions have been used to explain higher methane selectivity in FT synthesis over small Co particles. First, high methane selectivity was attributed to the sites of weak carbon monoxide adsorption (51). It is generally assumed that heavier hydrocarbons are favored when carbon monoxide and intermediates are strongly adsorbed by metal sites.

Second, Reuel and Bartholomew (16) assigned higher methane selectivity observed on well-dispersed low loading cobalt catalysts to the presence of stable unreduced oxide phases capable of catalyzing water-gas shift reaction: $CO + H_2O \rightarrow CO_2 + H_2$, and thereby increasing the H_2/CO ratio at the catalyst surface. The water-gas shift reaction suggests the emission of measurable amounts of carbon dioxide. Our data do not agree with this interpretation of higher methane selectivities on narrow pore catalysts, since carbon dioxide was not detected among reaction products.

Third, diffusion limitations for carbon monoxide in catalyst pores could also increase H_2/CO ratio in catalyst pore and thus, methane selectivities (13). It is known however, that an increase in effective H_2/CO ratio usually leads to both an increase in methane selectivity and to higher chain termination probability and to lower coefficient of chain propagation α. Table 3 shows that the decrease in pore sizes results only in higher methane selectivity, whereas the coefficient of chain propagation seems not to be affected by variation in catalyst pore diameters.

Our catalytic results (Table 3) also show that lower C_{5+} selectivity observed on narrow pore samples is likely to be related not to lower probability of chain propagation of narrow pore silicas, but to higher methane selectivity. Therefore, the contribution of mass transport limitations to higher methane selectivities observed on narrow pore catalysts is unlikely to be significant.

Analysis of literature data (16, 51) shows that higher methane selectivies are observed in FT synthesis when Co catalysts are not completely reduced or contain smaller cobalt particles. Figure 10 shows a relationship between

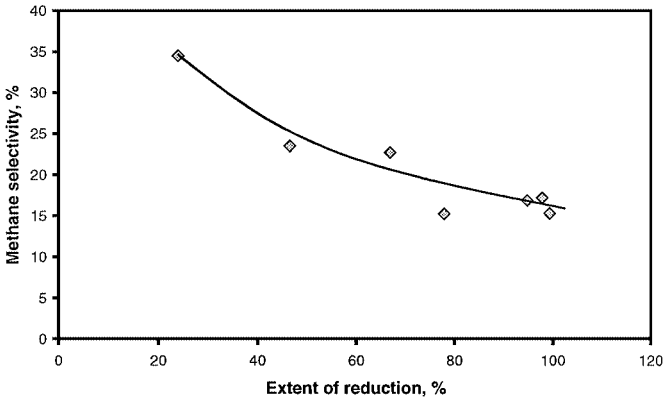

FIG. 10. Relation between methane selectivity and extent of the overall catalyst reduction.

methane selectivity and the extent of overall reduction of cobalt supported mesoporous silicas, higher methane selectivies being observed over less reduced samples. Note that such catalysts are always found to contain smaller Co_3O_4 particles (Table 2). Thus, higher methane selectivities observed on narrow pore silicas are likely to be attributed to the presence of either unreduced cobalt species or the small cobalt particles, which produce higher relative amounts of methane than large cobalt particles, rather than to either higher H_2/CO ratio in catalyst pores due to the water-gas shift reaction or diffusion limitations for carbon monoxide.

In the present work, catalytic behavior of Co supported catalysts was studied at atmospheric pressure and at low conversion levels. Higher pressures and higher carbon monoxide conversions would probably lead to the saturation of catalyst pores by liquid reaction products. The concentrations of hydrocarbons adsorbed in catalyst pores, especially the heaviest ones, depend on their partial pressure in the catalyst bed. The partial pressure of the products at the same conversion and selectivity levels depends on the total pressure in the reactor. An increase in total pressure even at the same conversions and selectivities could result in condensation of hydrocarbons, which are normally in the gaseous state at atmospheric pressure.

In addition, the partial pressure of reaction products depends on their yields. It is known (2, 17) that the reactant pressure in Fischer Tropsch synthesis affects usually chain growth and chain termination probabilities as well as the rates of secondary reactions. Iglesia, for example, showed (17) that chain termination probability to paraffin on Co/TiO_2 catalysts dramatically decreased as the reactant pressure increased from 540 to 2000 kPA. Higher chain growth probability leads to higher heavier hydrocarbon selectivities and therefore to higher yields of heavier hydrocarbons at higher reactant pressures even at the same carbon monoxide conversion. A simple increase in carbon

monoxide conversion levels with the same α would lead to higher yields of heavier hydrocarbons.

Thus, concentrations of heavier hydrocarbons in the catalyst pores and therefore mass transfer limitations could be much more severe at higher total pressures and at higher carbon monoxide conversions than at atmospheric pressure and low carbon monoxide conversions.

CONCLUSIONS

Catalytic and characterization results show strong impact of support porosity on the structure, reducibility, and FT catalytic behavior of cobalt species supported by mesoporous silicas.

Characterization techniques uncover that both the size of supported Co_3O_4 crystallites and their reducibility strongly depend on the pore diameter of mesoporous silicas. Small pores present in MCM-41 materials lead to a smaller size of the supported Co clusters and to their lower reducibility in hydrogen.

Catalytic experiments show that Co species located in the narrow pore silicas are much less active in Fischer Tropsch synthesis and produce methane with selectivities higher than larger cobalt particles in the wide pore supports. Lower FT activities and higher methane selectivities observed on the narrow pore cobalt catalysts are principally attributed to the lower reducibility of small cobalt particles.

ACKNOWLEDGMENTS

The authors gratefully acknowledge the help of C. Guelton in TGA measurements. We thank L. Gengembre for assistance with XPS, and A. J. Evans and N. B. Dinsdale for their help with Si1 and Si3 sample preparation. Thanks are due to F. DiRenzo for fruitful discussions and high expertise in the chemistry of mesoporous silicas.

REFERENCES

1. Thayer, A. M., *Chem. Eng. News,* March 13, 20 (2000).
2. Chaumette, P., *Revue IFP* **51**, 711 (1996).
3. Batley, G. E., Ekstrom, A., and Johnson, D. A., *J. Catal.* **34**, 368 (1974).
4. Guczi, L., Hoffer, T., Zsoldos, Z., Zyade, S., Maire, G., and Garin, F., *J. Phys. Chem.* **85**, 802 (1991).
5. van't Blik, H. F. J., Koningsberger, D. C., and Prins, R. J., *J. Catal.* **97**, 210 (1986).
6. van't Blik, H. F. J., and Prins, R., *J. Catal.* **97**, 188 (1986).
7. Schanke, D., Vada, S., Blekkan, E. A., Hilmen, A. M., Hoff, A., and Holmen, A., *J. Catal.* **156**, 85 (1995).
8. Eliason, S. A., and Bartholomew, C. H., *Appl. Catal. A: General* **186**, 229 (1999).
9. Li, J., and Coville, N. J., *Appl. Catal. A: General* **181**, 201 (1999).
10. Idem, R. O., Katikaneni, S. P. R., Sethuraman, R., and Bakhshi, N. N., *Energy and Fuels* **14**, 1072 (2000).
11. Ji, Y.-Y., Xiang, H.-W., Yang, J.-L., Xu, Y.-Y., Li, Y.-W., and Zhong, B., *Appl. Catal. A: General* **214**, 77 (2001).
12. Tihay, F., Pourroy, G., Richard-Plouet, M., Roger, A. C., and Kiennemann, A., *Appl. Catal. A: General* **206**, 29 (2001).
13. Anderson, R. B., Hall, W. K., Krieg, A., and Seligman, B., *J. Am. Chem. Soc.* **71**, 183 (1949).
14. Lapszewicz, J. A., Loeh, H. J., and Chipperfield, J. R., *J. Chem. Soc., Chem. Commun.* 913 (1993).
15. Vanhove, D., Zhuyong, Z., Makambo, L., and Blanchard, M., *Appl. Catal.* **9**, 327 (1984).
16. Reuel, R. C., and Bartholomew, C. H., *J. Catal.* **85**, 78 (1984).
17. Iglesia, E., Reyes, S. C., Madon, R. J., and Soled, S. L., *Adv. Catal.* **39**, 221 (1993).
18. Iglesia, E., Soled, S. L., and Fiato, R. A., *J. Catal.* **137**, 212 (1992).
19. Kresge, C. T., Leonowicz, M. E., Roth, W. J., Vartuli, J. C., and Beck, J. S., *Nature* **359**, 710 (1992).
20. Beck, J. S., Vartuli, J. C., Roth, W. J., Leonowicz, M. E., Kresge, C. T., Schmitt, K. D., Chu, C. T.-W., Olson, D. H., Sheppard, E. W., McCullen, S. B., Higgins, J. B., and Schlenker, J. L., *J. Am. Chem. Soc.* **114**, 10,834 (1992).
21. Matthae, F. P., Genske, D., Minchev, C., and Lechert, H., *Stud. Surf. Sci. Catal.* **117**, 223 (1998).
22. Chen, C.-Y., Li, H.-X., and Davis, M. E., *Microporous Mater.* **2**, 17 (1993).
23. Zholobenko, V. L., Evans, A., Plant, D., and Holmes, S. M., *Microporous Mesoporpous Mater.* **44–45**, 793 (2001).
24. Zhao, D., Feng, J., Huo, Q., Melosh, N., Fredrickson, G. H., Chmelka, B. F., and Stucky, G. D., *Science* **279**, 548 (1998).
25. Luan, Z., Hartmann, M., Zhao, D., Zhou, W., and Kevan, L., *Chem. Mater.* **11**, 1621 (2000).
26. Zhao, D., Sun, J., Li, Q., and Stucky, G. D., *Chem. Mater.* **12**, 275 (2000).
27. Barrett, E. P., Joyner, L. G., and Halenda, P. P., *J. Am. Chem. Soc.* **73**, 373 (1951).
28. Cullity, B. D., "Elements of X-ray Diffraction." Addision-Wesley, London, 1978.
29. Bechara, R., Balloy, D., Dauphin, J.-Y., and Grimblot, J., *Chem. Mater.* **11**, 1703 (1999).
30. Castner, D. G., Watson, P. R., and Chan, I. Y., *J. Phys. Chem.* **94**, 819 (1990).
31. Khodakov, A. Yu, Lynch, J., Bazin, D., Rebours, B., Zanier, N., Moisson, B., and Chaumette, P., *J. Catal.* **168**, 16 (1997).
32. Ernst, B., Bensaddik, A., Hilaire, L., Chaumette, P., and Kiennemann, A., *Catal. Today* **39**, 329 (1998).
33. Kerkhof, F. P. J., and Moulijn, J. A., *J. Phys. Chem.* **83**, 1612 (1979).
34. Seah, M. P., and Dench, W. A., *Surf. Interface Anal.* **1**, 2 (1979).
35. Scofield, J. H., *J. Electron Spectrosc.* **8**, 129 (1976).
36. Gregg, S. J., and Sing, K. S. W., "Adsorption, Surface Area and Porosity," second ed. Academic Press, New York, 1982.
37. Brunauer, S., Deming, L. S., Deming, W. S., and Teller, E., *J. Am. Chem. Soc.* **62**, 1723 (1940).
38. De Boer, J. H., *in* "The Structure and Properties of Porous Materials" (D. H. Everett and F. S. Stone, Eds.), pp. 68–94. London, Butterworths, 1958.
39. Bessell, S., *Appl. Catal.* **96**, 253 (1993).
40. Dimitrova, P. G., and Mehandjiev, D. R., *J. Catal.* **145**, 356 (1994).
41. Bessell, S., *Appl. Catal. A* **126**, 235 (1995).
42. Kerkhof, F. P. J., Moulijn, J. A., and Heeres, A., *J. Electron Spectrosc. Relat. Phenom.* **14**, 453 (1978).
43. Miller, M. L., and Linton, R. W., *Anal. Chem.* **57**, 2314 (1985).
44. Khodakov, A. Y., Griboval, A., Bechara, R., and Villain, F., *J. Phys. Chem. B* **105**, 9805 (2001).
45. Bonnelle, J. P., Grimblot, J., and D'huysser, A., *J. Electron Spectrosc.* **7**, 151 (1975).
46. Ho, S. W., Horialla, M., and Hercules, D. M., *J. Phys. Chem.* **94**, 6396 (1990).

47. Castner, D. G., Watson, P. R., and Chan, I. Y., *J. Phys. Chem.* **93**, 3188 (1989).
48. Ganesan, P., Kuo, H. K., Saaverda, A., and DeAngelis, R. J., *J. Catal.* **52**, 319 (1978).
49. Sun, S., Tsubaki, N., and Fujimoto, K., *Appl. Catal. A: General* **202**, 121 (2000).
50. Bartholomew, C. H., and Farrauto, R. J., *J. Catal.* **45**, 41 (1976).
51. Fu, L., and Bartholomew, C. H., *J. Catal.* **92**, 376 (1985).
52. Flory, P. J., *J. Am. Chem. Soc.* **58**, 1877 (1936).
53. Zhang, W.-H., Shi, J.-L., Chen, H.-R., Hua, Z.-L., and Yan D.-S., *Chem. Mater.* **13**, 648 (2001).
54. Iwamoto, M., Abe, T., and Tachibana, Y., *J. Mol. Catal. A: Chemical* **155**, 143 (2000).
55. Han, Y.-J., Kim, J. M., and Stucky, G. D., *Chem. Mater.* **12**, 2068 (2000).
56. Liu, Z., Sakamoto, Y., Ohsuna, T., Hiraga, K., Terasaki, O., Ko, C. H., Shin, H. J., and Ryoo, R., *Angew. Chem. Int. Ed.* **39**, 3107 (2000).